chemosensors

MDPI

Article

Enhancement of H_2 Gas Sensing Using Pd Decoration on ZnO Nanoparticles

Jin-Young Kim [1,2,†], Kyeonggon Choi [1,3,†], Seung-Wook Kim [1], Cheol-Woo Park [3], Sung-Il Kim [3], Ali Mirzaei [4,*], Jae-Hyoung Lee [5,*] and Dae-Yong Jeong [1,*]

[1] Department of Materials Science and Engineering, Inha University, Incheon 22212, Republic of Korea; piadote@hanyang.ac.kr (J.-Y.K.); kchoi10@hawk.iit.edu (K.C.); 22211581@inha.edu (S.-W.K.)
[2] The Research Institute of Industrial Science, Hanyang University, Seoul 04763, Republic of Korea
[3] Corning Technology Center Korea (CTCK), Asan 31454, Republic of Korea; parkc6@corning.com (C.-W.P.); kims24@corning.com (S.-I.K.)
[4] Department of Materials Science and Engineering, Shiraz University of Technology, Shiraz 71557-13876, Iran
[5] Electronic Materials Research Center, Korea Institute of Science and Technology, Seoul 02792, Republic of Korea
* Correspondence: mirzaei@sutech.ac.ir (A.M.); jhlee619@gmail.com (J.-H.L.); dyjeong@inha.ac.kr (D.-Y.J.)
† These authors contributed equally to this work.

Abstract: Hydrogen (H_2) gas, with its high calorimetric combustion energy and cleanness, is a green source of energy and an alternative to fossil fuels. However, it has a small kinetic diameter, with high diffusivity and a highly explosive nature. Hence, the reliable detection of H_2 gas is essential in various fields such as fuel cells. Herein, we decorated ZnO nanoparticles (NPs) with Pd noble metal NPs, using UV irradiation to enhance their H_2 gas-sensing performance. The synthesized materials were fully characterized in terms of their phases, morphologies, and chemical composition. Then, the sensing layer was deposited on the electrode-patterned glass substrate to make a transparent sensor. The fabricated transparent gas sensor was able to detect H_2 gas at various temperatures and humidity levels. At 250 °C, the sensor exhibited the highest response to H_2 gas. As a novelty of the present study, we successfully detected H_2 gas in mixtures of H_2/benzene and H_2/toluene gases. The enhanced H_2 gas response was related to the catalytic effect of Pd, the formation of heterojunctions between Pd and ZnO, the partial reduction of ZnO to Zn in the presence of H_2 gas, and the formation of PdH_x. With a high performance in a high response, good selectivity, and repeatability, we believe that the sensor developed in this study can be a good candidate for practical applications where the detection of H_2 is necessary.

Keywords: H_2 gas; Pd; ZnO; selectivity; gas sensor; sensing mechanism

Citation: Kim, J.-Y.; Choi, K.; Kim, S.-W.; Park, C.-W.; Kim, S.-I.; Mirzaei, A.; Lee, J.-H.; Jeong, D.-Y. Enhancement of H_2 Gas Sensing Using Pd Decoration on ZnO Nanoparticles. *Chemosensors* **2024**, *12*, 90. https://doi.org/10.3390/chemosensors12060090

Received: 15 April 2024
Revised: 21 May 2024
Accepted: 26 May 2024
Published: 27 May 2024

1. Introduction

Nowadays, because of extensive air pollution, mainly due to the emission of toxic gases from burning of fossil fuels, many research teams are widely investigating alternative eco-friendly energy sources [1,2]. Hydrogen (H_2) is one of the most promising green energy resources that can replace fossil fuels. It has a high energy content per unit mass, making it a potent alternative fuel [3]. This characteristic is especially advantageous for applications such as transportation, where weight is a critical factor. In addition, hydrogen produces water by reacting with oxygen and does not produce polluting emissions when used as an energy source [4]. Accordingly, hydrogen has been actively investigated for use in different fields, such as automobiles, aerospace, fuel cells, and power plants [5–7]. Nevertheless, the high diffusion coefficient of hydrogen (0.61 cm^2/s) [8], and its small diameter (~0.29 nm) [9], result in rapid diffusion in the air in the case of gas cylinder leakage. Because of its highly explosive characteristics, a low explosive limit of 4.0 vol%, a high heat of combustion, a rapid flame propagation velocity, and low ignition energy, the release of this explosive

gas can result in catastrophic accidents [10–12]. Furthermore, its colorless and odorless properties render it insensible to humankind, emphasizing the need for advanced and highly efficient hydrogen-sensing devices capable of detecting low concentrations of this gas. This is essential for preventing potential hazardous accidents and explosions [13–15].

Gas sensors are electronic devices which respond to the variations of composition of gases in their surrounding atmosphere by the generation of an electronic signal that is proportional with the concentration of the target gas. Many researchers have investigated various types of H_2 gas sensors, such as electrochemical [16], surface acoustic wave (SAW) [17], optical fiber [18], piezoelectric [19], and resistive types in laboratories, as well as in real applications. The latter ones are nowadays highly popular, thanks to their high sensitivity, good stability, fast dynamics, simple design and construction, and low price. They are mostly fabricated from n-type semiconducting metal oxides such as ZnO [20–22], SnO_2 [23,24], TiO_2 [25,26], and WO_3 [27,28], thanks to their favorable band gaps and high mobility of charge carriers. The general sensing mechanism of resistive gas sensors is based on variations of the electrical resistance in the presence of target gases. Since in this type of gas sensor, the response depends on amounts of adsorbed gas on the sensor surface, different morphologies of metal oxides such as nanorods, nanotubes, nanowires, nanofibers, and nanoparticles (NPs) have been reported for gas-sensing applications. Nowadays, resistive gas sensors play a significant role in addressing various industrial, environmental, and safety challenges, making them a focal point for research and development in gas-sensing technologies.

ZnO with n-type conductivity and a bandgap of 3.37 eV has a high mobility of electrons, nontoxicity, high chemical and physical stability, ease of synthesis, high availability, and a low price, and it is a well-known semiconducting metal oxide that shows a phase transition when interacting with H_2 gas molecules at high temperatures [29–31]. However, two main problems associated with the ZnO gas sensor are the high sensing temperature and poor selectivity. High sensing temperatures lead to high power consumption, which ultimately can limit the application of the sensor in remote areas or places with a shortage of energy. Also, poor selectivity can lead to false alarms and problems with the reliability of the sensor. Accordingly, some strategies have been proposed to enhance the overall performance of ZnO gas sensors, especially in terms of sensing temperatures and selectivity.

One of the most promising techniques to boost the sensing performance of resistive gas sensors is decoration with noble metals such as Au, Ag, Pt, Ru, and Pd. Among them, the Pd noble metal demonstrates excellent catalytic effects towards H_2 gas [32,33]. Due to the catalytic properties of Pd, hydrogen molecules undergo decomposition into H atoms on the surfaces of Pd. Then, due to the spillover effect, decomposed H atoms migrate to the surfaces of sensing materials, where they will eventually be adsorbed. This adsorption triggers a reaction with oxygen species on the semiconducting sensing layer, resulting in a change in electrical resistance and the generation of a sensing signal [34]. Besides, Pd can adsorb an extensive amount of H_2 gas, changing to PdH_x, with quite different electrical properties than pure Pd. It is already reported that the decoration of catalyst metal particles such as Pd could enhance the gas-sensing properties of semiconducting materials [34]. Thus, it seems that Pd decoration on ZnO NPs can be a good strategy to boost their sensing response towards H_2 gas.

In this study, we decorated the surface of ZnO NPs with Pd NPs using a UV irradiation procedure at room temperature. The synthesized materials were fully characterized in terms of their phase, morphology, and chemical composition. Based on H_2 gas-sensing studies, Pd decoration on ZnO led to an enhanced response to H_2 gas. The optimized gas sensor, designed to integrate seamlessly with transparent devices based on semiconductor technology, holds the potential for practical applications in electronic devices requiring hydrogen sensing.

2. Materials and Methods

2.1. Materials

In this study, we used Corning EXG (150 × 150 mm^2) with a thickness of 0.5 mm as a gas sensor substrate. Commercially available ZnO NPs (Sigma-Aldrich, Germany) were used for fabricating the sensing layer, while palladium chloride ($PdCl_2$) was used for the decoration of the ZnO.

2.2. Synthesis of the Pd-Decorated ZnO NPs

Initially, 0.017 g of $PdCl_2$ was dissolved into a mixed solvent comprising 8.5 g of 2-propanol and 8.5 g of acetone. Later on, 0.05 g of ZnO NPs was added to the above solution under constant stirring. UV light was used for the reduction of Pd^{2+} ions as Pd NPs on the surface of ZnO NPs as decoration. To this end, the solution containing ZnO and $PdCl_2$ was exposed to UV light with a fixed intensity of 0.11 mW/cm^2 for 15 s. The UV-irradiated products were carefully collected by filtering, and finally they were annealed at 600 °C for 1 h to achieve crystalline products without any residue. Scheme 1a schematically presents the synthesis procedure of Pd-decorated ZnO NPs.

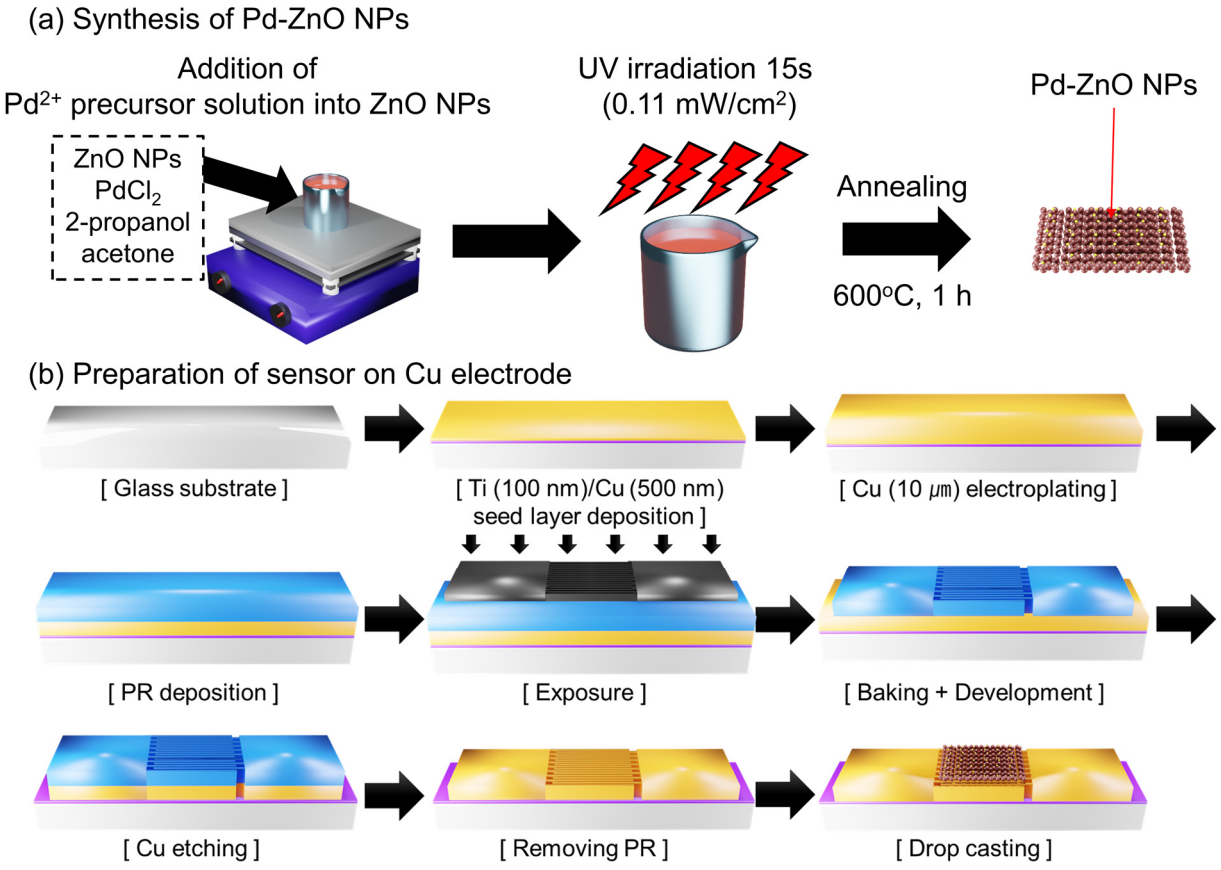

Scheme 1. (**a**) Schematic of synthesis of Pd-decorated ZnO NPs; (**b**) preparation of gas sensor on glass substrate equipped with Cu electrodes.

2.3. Preparation of Glass Substrate

At first, Ti (100 nm) and Cu (500 nm) seed layers were deposited on the prepared Corning EXG glass. Subsequently, electroplating processes were performed before pattern fabrication, where Cu with a thickness of 10 µm was deposited over the substrate. Following this, using a photolithography process, Cu patterns were created over the substrate (Scheme 1b). It should be mentioned that the pattern size was 10 µm to fabricate an electrode.

2.4. Gas-Sensing Measurements

The as-synthesized Pd-decorated ZnO NPs were deposited on the glass substrate with Cu electrodes for gas-sensing studies. The synthesized Pd-ZnO powders were dissolved in DI water at a ratio of 1:10 (milliliter and microliter units). Then, using a micropipette, the mixed powder was dropped (three droplets; ~0.01 µL) on the sensor substrate. Finally, it was dried in air at 60 °C. On each substrate, we fabricated one sensor by the deposition of the sensing layer over it. Due to employing a simple drop casting method for the deposition of the sensing layer, the yield and throughput of sensor fabrication was high, without any waste material.

Gas sensing measurement was performed as follows. The target gas concentration was 100 parts per million (ppm) in cylinders with dry air without relative humidity (0% RH) conditions. We used dry air as a balancing gas to produce target gases (H_2, C_7H_8, C_6H_6, CO, and C_2H_5OH) at the desired concentration. Using mass flow controllers (MFCs), dry air-balanced target gas from standard cylinders and pure dry air were combined in a desired ratio and injected into the gas chamber to achieve the target gas concentration. A constant flow rate of 500 cm was kept throughout the sensing measurements. For the sensing tests, using a Keithley 2400 source meter, the sensor's resistance in the air (R_a) and in the presence of the target gas (R_g) were constantly measured, and the sensor response was calculated as $R = R_a/R_g$. The response time and recovery times are defined as the time taken for the sensor to reach 90% of its total resistance change to the presence and stoppage of H_2 gas, respectively. H_2 gas-sensing behaviors were tested at various temperatures in both dry and humid air (RH 0–80%). To test the sensor behavior in the presence of RH, dry air was injected into a sealed gas beaker filled with water to prepare the air to 100% RH. This created air bubbles that flowed into the exit line. The RH values could be adjusted by combining dry air with 100% humid air.

2.5. Materials Characterization

X-ray diffraction (XRD; Philips X'pert MRD) using CuKα radiation (1.5406 Å) was used to examine the crystallinity and phase formation of the synthesized materials. The voltage and tube current were fixed at 40 V and 30 A, respectively. The sample was scanned in the range of 2θ = 20 to 80°, with a step size of 0.05° and a scan speed of 0.05°/s. The morphological features were examined via both field-emission scanning electron microscopy (FE-SEM, Hitachi-S-4200) and transmission electron microscopy (TEM, JEOL Ltd., Tokyo, Japan, JEM-3010). The elemental composition and chemical states were examined via X-ray photoelectron spectroscopy (XPS, VG Multitab ESCA2000) using a monochromatized Al Ka X-ray source (hν = 1486.6 eV). The C1s peak position (284.5 eV) was used to calibrate the XPS peaks.

3. Results and Discussion

3.1. Morphological and Chemical Studies

Figure 1 presents XRD patterns of Pd-decorated ZnO NPs. The (100), (002), (101), (102), (110), (103), (200), (112), (201), (004), and (202) peaks are matched with JCPDS File No 89-0510, belonging to crystalline ZnO with a hexagonal Wurtzite crystal structure. Also, a small peak related to (220), the crystalline plane of Pd (JCPDS File No. 05-0681) with a face-centered cubic (FCC) crystal structure, can be seen. It should be noted that due to the small amount of Pd NPs, the peak related to Pd has a very low intensity, and the presence of Pd should be also approved by other techniques.

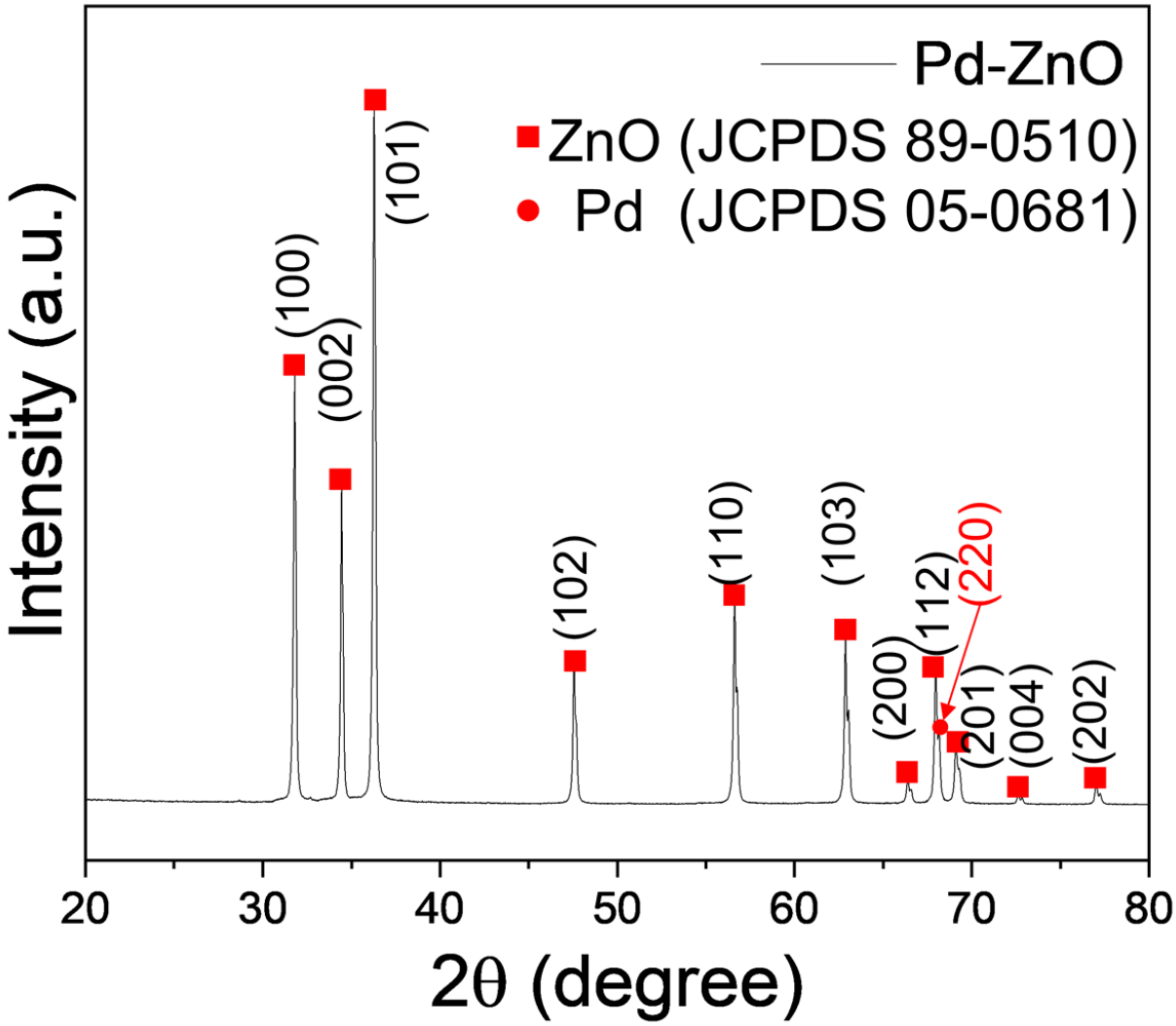

Figure 1. XRD pattern of Pd-decorated ZnO NPs.

Figure 2a presents a typical SEM image of Pd-decorated ZnO NPs, in which almost spherical particles can be easily seen. Most of the ZnO NPs have sizes less than 100 nm. We performed a SEM-EDS analysis to check their chemical composition (Figure 2b). Weight percentages of O, Zn, and Pd were 21.23, 77.32, and 1.45, respectively, demonstrating the presence of a small amount of Pd as a decoration on the surface of the ZnO NPs. In the next step, we carried out a TEM analysis to see the presence of Pd NPs. Figure 2c offers a typical TEM image, showing the presence of small Pd NPs on the surface of ZnO NPs. Also, in Figure 2d, a typical HRTEM is presented, demonstrating the crystalline nature of the synthesized materials. Figure 2e–h display a TEM-EDS elemental color mapping of Pd-decorated ZnO NPs, in which the concentrations of O and Zn elements are high, demonstrating the co-existence of Zn and O as a ZnO phase. Also, the Pd element with a lower concentration is dispersed on the surface of the ZnO. Thus, based on the above characterization analyses, it can be concluded that pure crystalline ZnO decorated with Pd NPs has been successfully formed. The thickness of the sensing film on the substrate was about 25 μm (Figure S1).

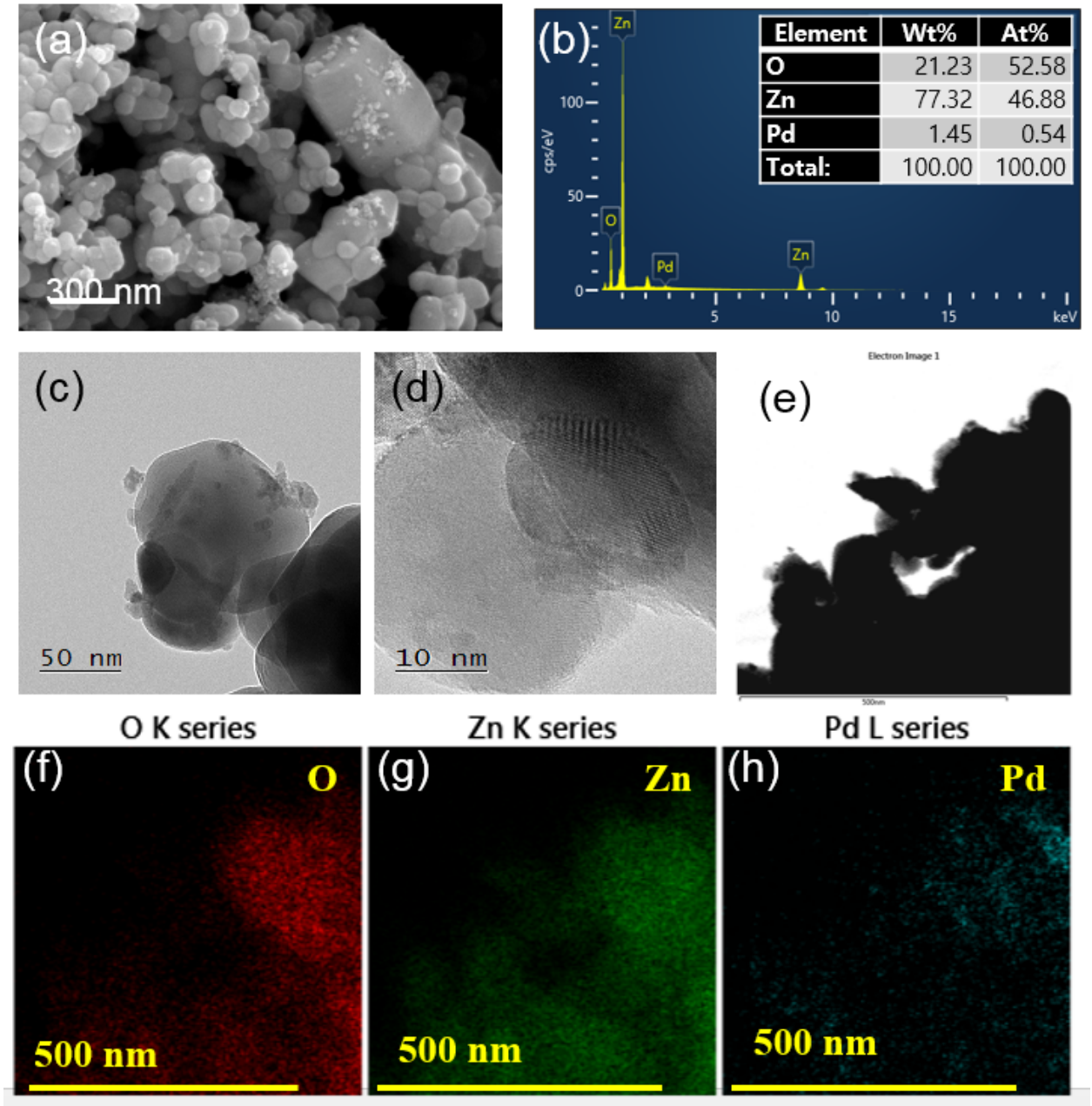

Figure 2. (**a**) SEM image of Pd-decorated ZnO NPs and (**b**) corresponding EDS analysis. (**c**) TEM and (**d**) HRTEM images of Pd-decorated ZnO NPs. (**e**–**h**) TEM-EDS color mapping analysis of Pd-decorated ZnO NPs.

Figure 3a offers an XPS survey of Pd-decorated ZnO NPs, in which the peaks related to the expected Zn, O, and Pd elements are observed without the presence of impurity peaks. This demonstrates the high purity of the synthesized materials. To have a better insight, we also have deconvoluted the core-level regions. Figure 3b presents the Zn 2p core-level region. Two prominent peaks at 1044.51 and 1021.41 eV were attributed to Zn $2p_{1/2}$ and Zn $2p_{3/2}$ of Zn^{2+} in the ZnO phase [35]. Figure 3c offers the O1s core-level region, which is deconvoluted into three curves located at 530.5 eV, 531.6 eV, and 532.6 eV, which can be related to the lattice oxygen (O_L), oxygen vacancy, and chemisorbed oxygen, respectively [36]. Both oxygen vacancy and adsorbed oxygen species are highly beneficial for adsorption and gas-sensing reactions on the sensor surface. Figure 3d presents the deconvoluted Pd 3d region, in which the peaks related to metallic Pd^0 and the oxidized form of Pd (PdO and PdO_2) can be seen. In fact, ultrafine Pd NPs can be easily and partially

oxidized in air to form both PdO and PdO_2 phases, which have quite different electrical features relative to Pd.

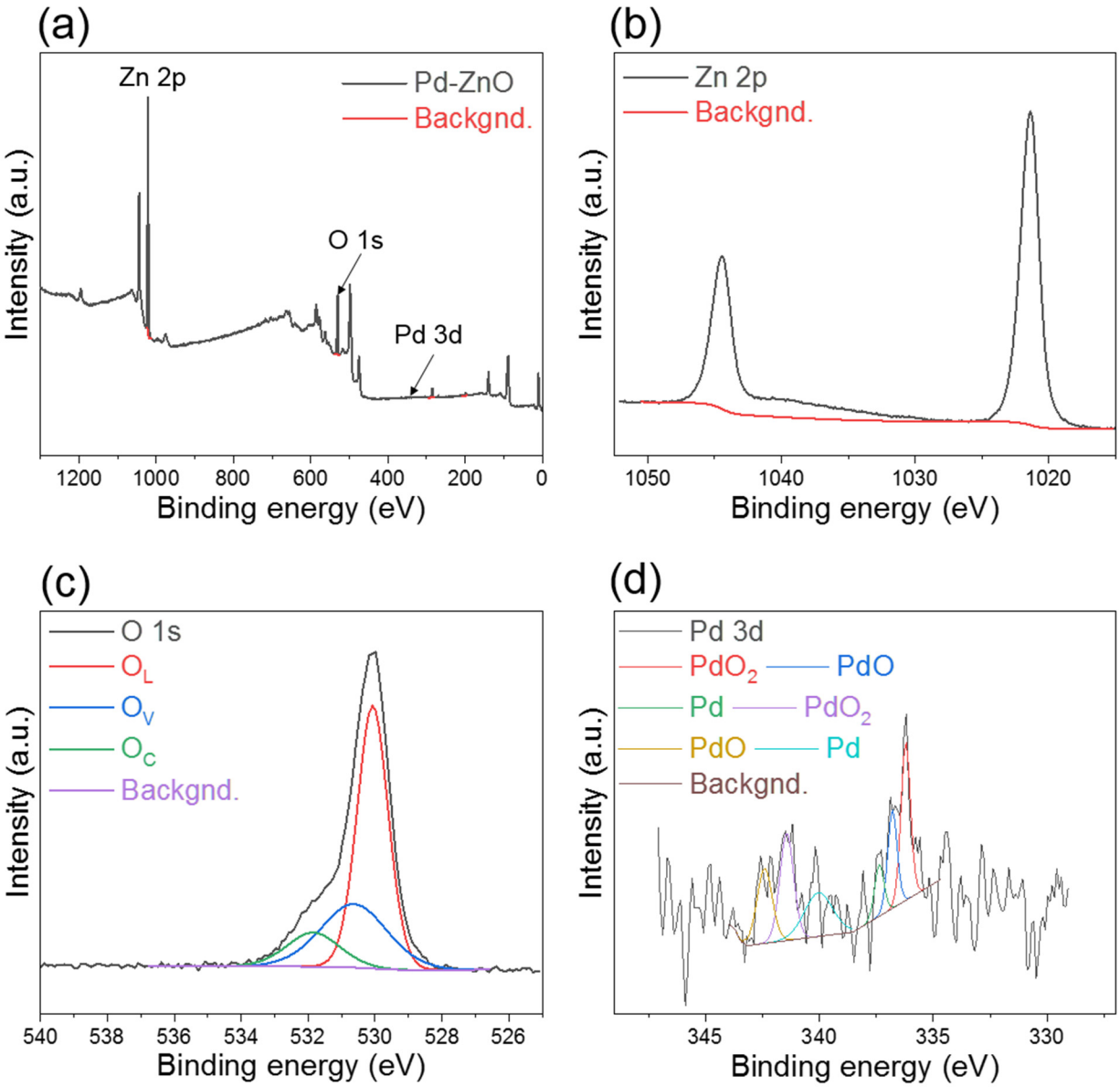

Figure 3. (**a**) XPS survey of Pd-decorated ZnO NPs and corresponding deconvoluted core-level XPS region of (**b**) Zn 2p, (**c**) O 1s, and (**d**) Pd 3d.

3.2. Gas-Sensing Studies

Figure 4a displays the dynamic resistance curves of Pd-decorated ZnO NPs to 10, 30, and 50 ppm H_2 gas at different temperatures (25–350 °C). At low temperatures (25 and 50 °C), the resistance is extremely high (in the range of tera-ohm), and no variation was recorded upon the injection of H_2 gas. By increasing the sensing temperature, the baseline resistance decreased gradually due to the jumping of electrons from the valence band to the conduction band of the ZnO. When the sensing temperature was 150 to 350 °C, the sensor was able to detect H_2 gas. All the resistance decreased upon exposure to H_2 gas, revealing the n-type nature of the ZnO gas sensor, as expected. Also, the resistance comes back to its initial value after the stoppage of H_2 gas, revealing the reversibility of the sensor. To gain a better insight, we calculated the response values versus sensing temperature for different concentrations of H_2 gas (Figure 4b). For all gas concentrations, the response value gradually increases up to 250 °C, and then it decreases. In fact, at low

temperatures, there is not sufficient energy for H_2 gas to surpass the adsorption barrier, while at high temperatures, the desorption rate is higher than the adsorption rate. At the optimal sensing temperature, the adsorption and desorption rates are equal, and maximum response is observed. Since at 250 °C, the sensor showed an enhanced response to H_2 gas, further studies were performed at 250 °C. To check the sensor properties in detail, we also investigated the baseline resistance at different temperatures (Figure 4b). The resistance values at 100, 150, 200, 250, 300, and 350 °C were ~560, 234, 42, 35.7, 4.3, and 0.77 MΩ, respectively. Thus, as expected, the resistance values decreased, which reflects the semiconducting nature of the sensing material. In addition, we calculated the response time and recovery time versus a high sensing temperature for different concentrations of H_2 gas (Figure 4c). Also, in Table S1, we have summarized the details of response time and recovery time.

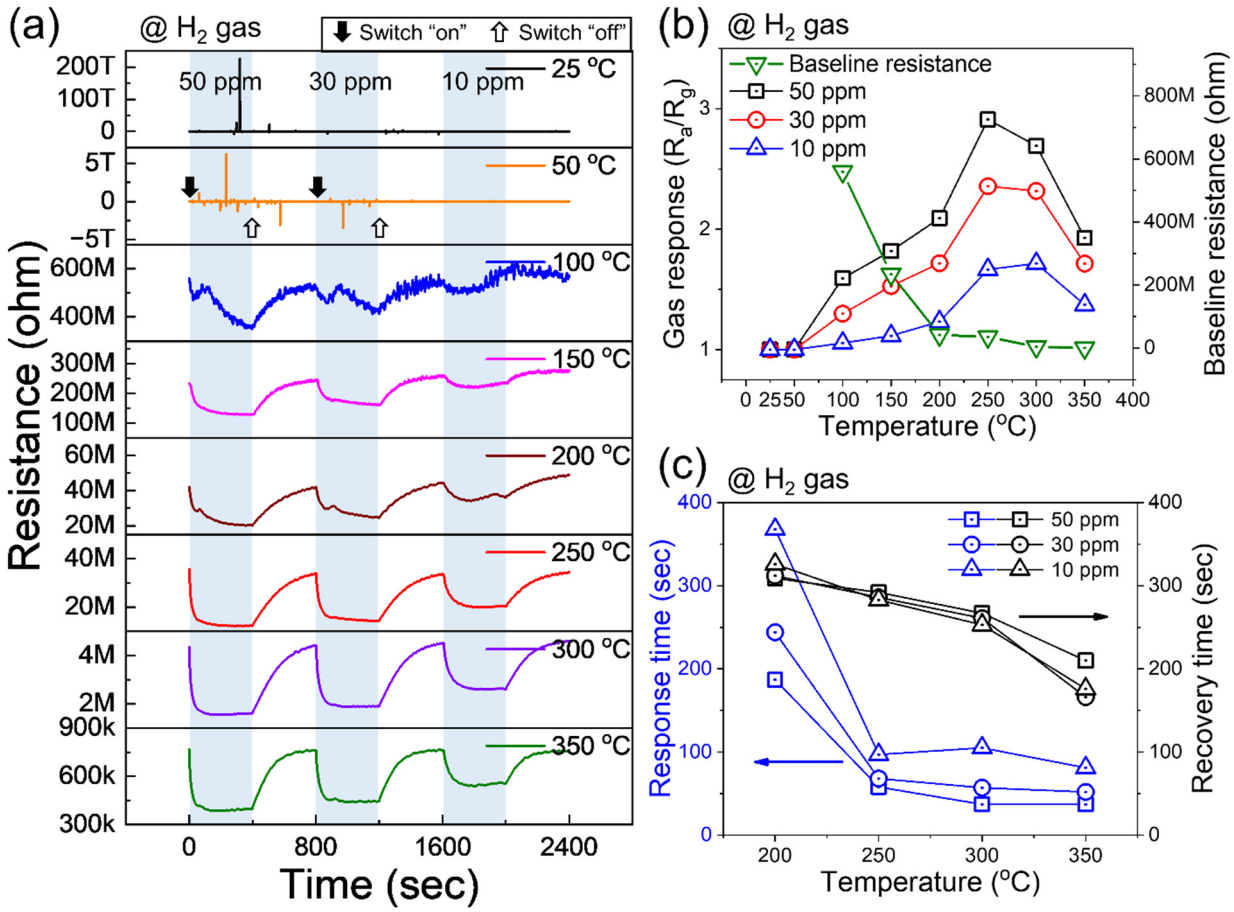

Figure 4. (**a**) Dynamic resistance curves of Pd-decorated ZnO NPs sensor to 10, 30, and 50 ppm H_2 gas at different temperatures. (**b**) Corresponding baseline resistance and gas response curve versus temperature at different H_2 gas concentrations. (**c**) Corresponding response and recovery time versus temperature at different H_2 gas concentrations.

Since the sensor exhibited the highest response at 250 °C, it was chosen as the optimal sensing temperature. It should be noted that at 350 °C, not only was the sensing response lower, but also, the operation of the sensor at a higher temperature leads to higher power consumption, which limits its application for remote areas. Therefore, other tests were performed at 250 °C.

Selectivity is one of the most important parameters of gas sensors. Selective behavior means having a high response to a specific gas, with no or a weak response to interfering gases. Obviously, high selectivity prevents false alarms and contributes to the greater reliability of the gas sensor. Accordingly, in the next step, we explored the selectivity

behavior of the Pd-decorated ZnO gas sensor at the optimal temperature. Figure 5a offers dynamic resistance graphs of Pd-decorated ZnO NPs to various concentrations of different gases (H_2, C_6H_6, C_7H_8, CO, and C_2H_5OH) at 250 °C, and Figure 5b displays corresponding calibration curves for various gases. The sensor exhibited a higher response to H_2 gas than other gases at all concentrations, demonstrating its high selectivity to H_2 gas, which is essential from a practical point of view.

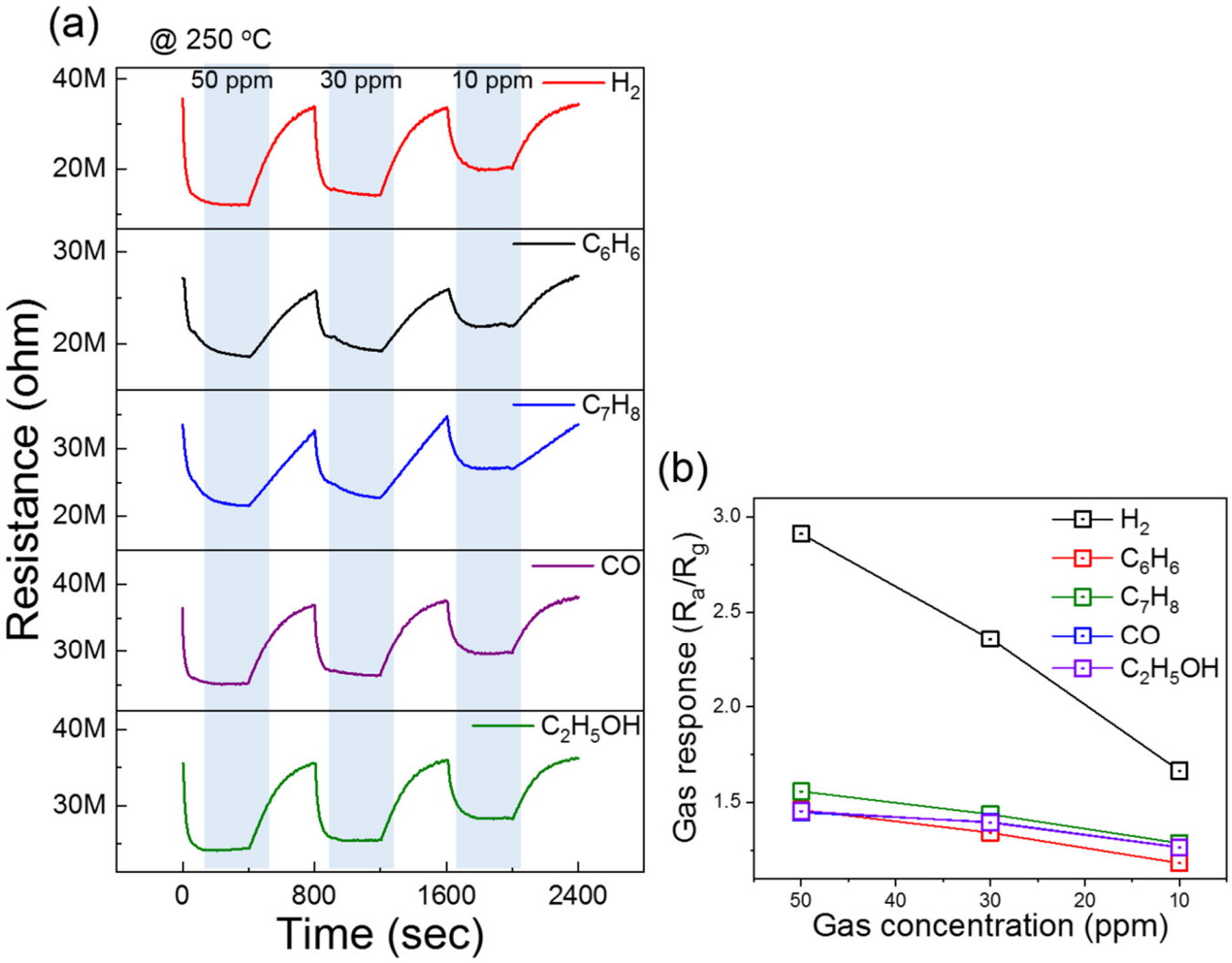

Figure 5. (**a**) Dynamic resistance curves of Pd-decorated ZnO NPs for various concentrations of different gases at 250 °C. (**b**) Corresponding gas response for various concentrations of different gases.

We also expanded the selectivity study to the mixture of gases, which may be encountered in real applications. Figure 6a presents dynamic resistance plots of the Pd-decorated ZnO NPs sensor to various concentrations of H_2, C_7H_8, and C_6H_6 gases and (H_2 + C_6H_6), (H_2 + C_7H_8), and (C_6H_6 + C_7H_8) gases at 250 °C. Figure 6b shows that the sensor responds more to H_2 gas than other gases and mixed gases. Even when C_6H_6 gas or C_7H_8 gas is mixed with H_2 gas, the response is increased due to the presence of H_2 gas; overall, the response is lower than to pure H_2 gas. This again demonstrates the high selectivity of the Pd-decorated ZnO NPs sensor to H_2 gas.

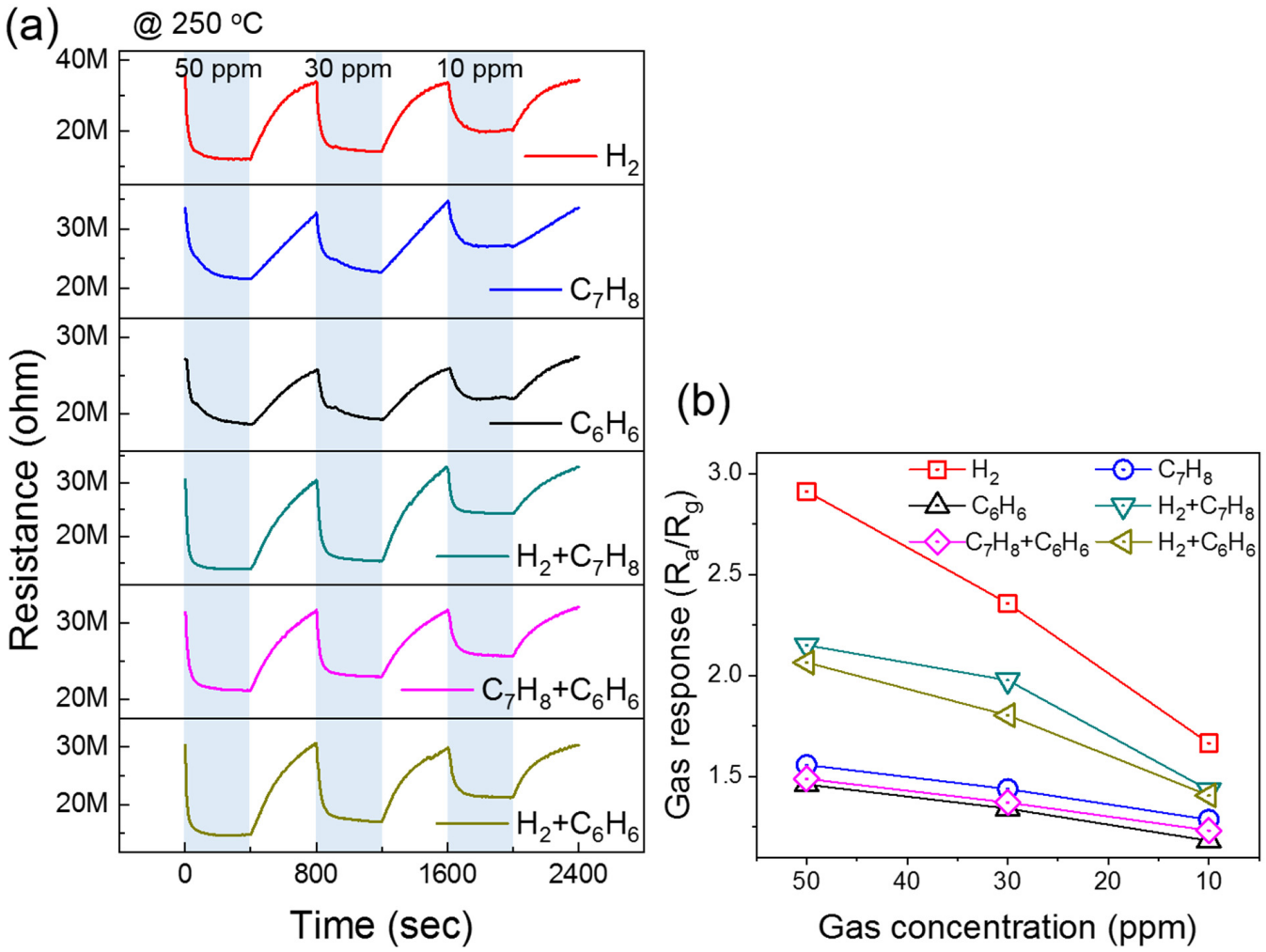

Figure 6. (**a**) Dynamic resistance curves of Pd-decorated ZnO NPs to various concentrations of H_2, C_7H_8, and C_6H_6 gases and their mixtures with H_2 gas at 250 °C. (**b**) Corresponding gas response for different gases and their mixtures.

We also checked the repeatability of the Pd-decorated ZnO gas sensor to 50 ppm H_2 gas at 250 °C during 12 sequential cycles (Figure 7a). The sensor showed almost the same sensing behavior, and as shown in Figure 7b, there are only negligible variations in the sensing response at different cycles, implying the excellent repeatability of the Pd-decorated ZnO gas sensor. Finally, we explored the sensing performance of the sensor to 50 ppm H_2 at 250 °C in the presence of various levels of RH (0, 20, 40, 60, and 80%), as shown in Figure 7c. By increasing the RH, the response to H_2 gas gradually decreased (Figure 7d). Indeed, in a humid environment, water molecules are adsorbed on the sensor surface, and hence, the number of available sensing sites decreases. Accordingly, less H_2 gas was adsorbed on the sensor relative to a dry environment. Accordingly, a lower response was recorded.

We also studied the stability of our sensor by exposing it to 50 ppm H_2 gas at 250 °C after 2, 4, and 12 weeks (Figure 8a). After two weeks, there is a negligible decrease in the response. Even though, after 4 and 12 weeks, the response is lower relative to a fresh sensor, the response is still acceptable (Figure 8b).

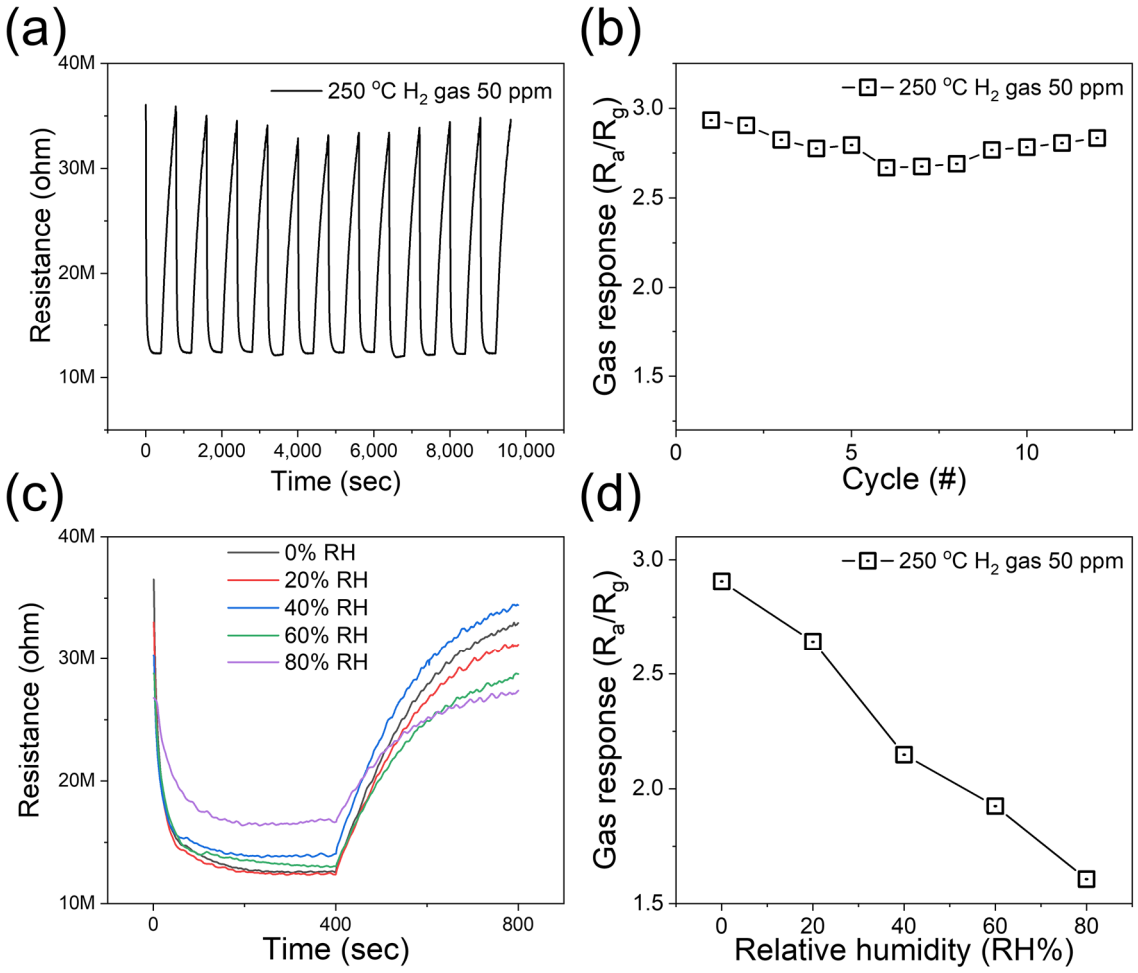

Figure 7. (**a**) Repeatability of Pd-decorated ZnO gas sensor during twelve H_2 sensing cycles (50 ppm) at 250 °C. (**b**) Corresponding response versus gas-sensing cycle number. (**c**) Dynamic resistance curves of Pd-decorated ZnO gas sensor to 50 ppm H_2 gas at 250 °C in presence of various levels of RH (0–80%). (**d**) Corresponding H_2 gas response versus RH (%).

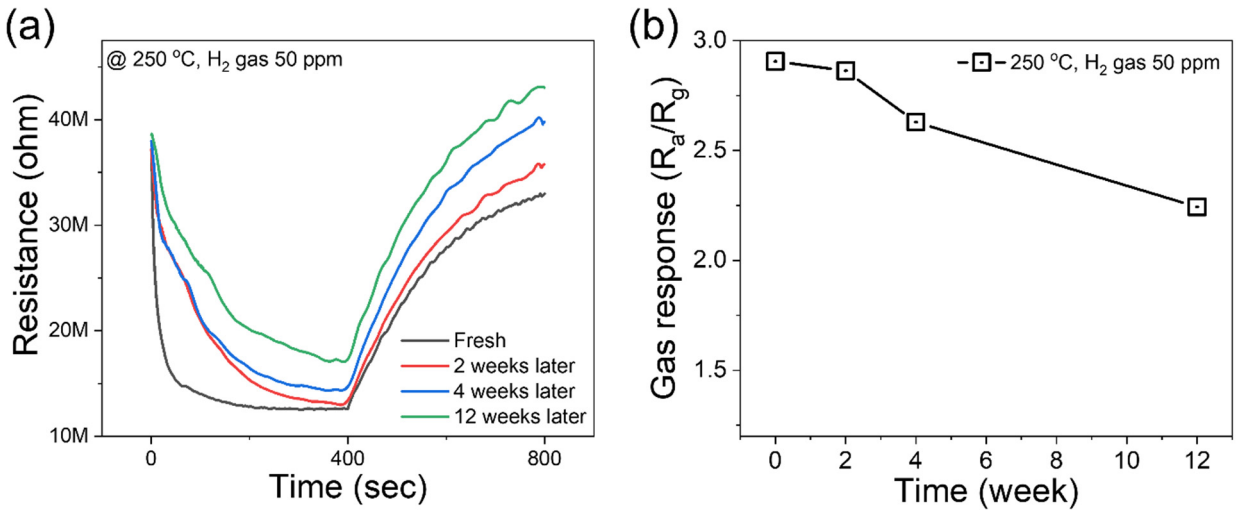

Figure 8. (**a**) Long-term stability of Pd-ZnO gas sensor dynamic resistance curves, (**b**) response values in fresh state and after 2, 4, and 12 weeks to 50 ppm H_2 gas at 250 °C.

We also annealed a Pd-ZnO sample at 300 °C (Figure S2a) for 4 h and then fabricated a sensor for H_2 gas sensing. It showed responses of 1.72, 2.01, and 2.10 to 10, 30, and 50 ppm H_2 gas at 250 °C (Figure S2b). Therefore, it revealed a lower sensing performance relative to the sensor annealed at 600 °C.

3.3. Gas Sensing Mechanism

In resistance gas sensors, the changes of electrical resistance in the presence of the target gas cause the generation of a sensing signal. When the sensor is exposed to fresh air, oxygen from the air is adsorbed on its surface, and due to the high electron affinity of oxygen, it becomes chemisorbed on the sensor surface by abstraction of electrons as follows:

$$O_2(g) \rightarrow O_2(ads) \quad (1)$$

$$O_2(ads) + e^- \rightarrow O_2^-(ads) \quad (2)$$

$$O_2^-(ads) + e^- \rightarrow 2O^-(ads) \quad (3)$$

$$O^-(ads) + e^- \rightarrow O^{2-} \quad (4)$$

Each reaction dominates at a particular temperature range; at the sensing temperature (250 °C), O^- is the dominant oxygen species. Accordingly, an electron depletion layer (EDL) is formed on the surface of the ZnO NPs. Since, in this layer, the concentration of electrons is lower relative to the core parts of the ZnO NPs, the formation of an EDL causes an overall increase in the sensor resistance relative to vacuum conditions [37]. Upon exposure to H_2 gas, the following reaction between H_2 and the adsorbed oxygen is likely [38]:

$$H_2 + O^- \rightarrow H_2O(g) + e^- \quad (5)$$

Hence, the electrons are liberated to the sensor surface, and the width of the EDL decreases. This causes a decrease in resistance upon exposure to H_2 gas. In addition, at contact points between ZnO-ZnO NPs, double Schottky barriers form in the air, creating barriers for the flow of electrons from one ZnO NP to the next one. Upon exposure to H_2 gas and the release of electrons, the height of the double Schottky barriers decreases, allowing more electrons to flow among neighboring ZnO NPs, resulting in a significant decrease in resistance.

Furthermore, the role of Pd should not be ignored. Pd is a well-known and highly efficient catalyst for H_2 dissociation. Accordingly, H_2 molecules can be easily adsorbed on the surface of Pd NPs and become dissociate to active atomic species as follows [39]:

$$H_2(g) \xrightarrow{Pd} H + H \quad (6)$$

In a so-called spillover effect, dissociated "H" species move to neighboring ZnO NPs, and subsequently, atomic "H" reacts with the adsorbed oxygen as follows [39]:

$$2H + O^- \rightarrow H_2O + e^- \quad (7)$$

Liberated electrons decrease the resistance of the sensor. Apart from the catalytic activity of Pd as described above, since some of the Pd NPs were converted to PdO and PdO_2 in air (as shown in the XPS analysis; Figure 3d), PdO-ZnO and PdO_2-ZnO heterojunctions initially form in air due to the difference between the work functions of PdO/PdO_2 and ZnO, which act as barriers to the flow of electrons. In the H_2 gas atmosphere, due to the highly reducing nature of H_2 gas, PdO and PdO_2 can be easily converted to metallic Pd with a quite different conductivity and work function than PdO and PdO_2. Thus, a significant modulation of barrier heights occurs, leading to a remarkable resistance modulation of the gas sensor [40]. Besides, Pd can adsorb a significant amount of H_2 gas, changing to PdH_x, with quite different electrical properties than pure Pd. Thus, this mechanism also can contribute to the sensing mechanism.

Another source of resistance modulation is the possible reduction of the surface of the ZnO to metallic Zn at sensing temperature (250 °C) upon exposure to H_2 gas, which has a highly reducing nature [29]. Since ZnO is a semiconductor and Zn has metallic conductivity, reducing ZnO to Zn results in a remarkable electrical resistance change. However, this reduction likely happens for ultrafine ZnO NPs with a high enough reactivity at sensing temperature.

Table 1 compares the gas-sensing properties of the present sensor with those reported in the literature. Overall, it can be seen that the present sensor exhibits a good performance relative to other listed sensors in terms of the relatively low sensing temperature and good response.

Table 1. Comparison of H_2 gas-sensing properties of present sensor with those reported in literature.

Sensing Materials	Conc. (ppm)	T (°C)	Gas Response (R_a/R_g) or (R_g/R_a)	τ_{res}/τ_{rec} (s)	Ref.
Pd-ZnO	50	250	2.94	58/292	Present Work
SnO_2 honeycomb	1	340	8.4	4/10	[41]
In_2O_3 nanocluster	500	400	18	1.7/1.5	[42]
Urchin-like WO_3 nanoparticles	50	250	~4	-/-	[43]
V_2O_5 hollow ano sphere	200	25	3.8	30/5	[44]
Fe_2O_3 nanotube	50	200	2.3	-/-	[45]
ZnO nanohexagone	10	175	1.089	11.5/14.5	[46]
PdO nanoflake	250	200	1.9	-/-	[47]
Pd-ZnO nanorods	250	135	22.5	1/52	[48]
Pd-WO_3 nanofibers	500	450	16.3	-/-	[49]
Pd-CuO nanorod	1000	200	4.5	600/960	[50]
Pd/SnO_2/RGO	5000	25	45.5%	>50/>1000	[51]
Si-Pd-Ni	200	70	2.21	107/-	[52]
Pd/WO_3	1000	300	1.184	5/6	[53]
Pd-Au	3000	60	1.033	22/160	[54]
TGS2616-C00	100	5 V	~20	-/-	[55]
GMV-2021B	200	2.5 V	>5	~20/~45	[56]

4. Conclusions

In a nutshell, Pd decoration on ZnO NPs was successfully performed using UV irradiation. Different characterizations such as XRD, SEM, and TEM demonstrated the successful formation of Pd-decorated ZnO with the desired phase, crystallinity, morphology, and chemical composition. A gas sensor on a glass substrate was fabricated and tested for H_2 gas. H_2 gas-sensing tests at various temperatures revealed that the best sensing performance occurred at 250 °C. Also, the sensor exhibited a good selectivity to H_2 gas, even in the presence of mixed (H_2 + C_6H_6), (H_2 + C_7H_8), and (C_6H_6 + C_7H_8) gases. Furthermore, it showed excellent repeatability during twelve sequential cycles. This enhanced H_2 gas-sensing performance was related to the promising effect of Pd, with catalytic activity on H_2 gas and electronic effects. Also, the surface reduction of ZnO to metallic Zn in the presence of H_2 gas contributed to the sensing signal. The present study highlights the promising effects of Pd decoration on ZnO NPs for enhanced H_2 gas sensing.

Supplementary Materials: The following supporting information can be downloaded at: https://www.mdpi.com/article/10.3390/chemosensors12060090/s1, Table S1: Response time and recovery time of the Pd-ZnO sensor at different temperatures towards various concentrations of H2 gas; Figure S1: Cross-sectional SEM image of Pd-ZnO on substrate.

Author Contributions: Conceptualization, D.-Y.J., J.-H.L. and A.M.; methodology, S.-I.K.; validation, K.C. and J.-Y.K.; formal analysis, C.-W.P. and J.-Y.K.; investigation, J.-Y.K., K.C. and S.-W.K.; data curation, J.-Y.K., K.C., S.-W.K. and S.-I.K.; writing—original draft preparation, K.C., A.M. and J.-H.L.; writing—review and editing, S.-I.K., D.-Y.J. and J.-H.L.; visualization, D.-Y.J., J.-H.L. and A.M.; supervision, D.-Y.J. and J.-H.L.; project administration, D.-Y.J. and J.-H.L.; funding acquisition, D.-Y.J. All authors have read and agreed to the published version of the manuscript.

Funding: This research was supported by Inha University. This work is not associated with Corning Incorporated.

Institutional Review Board Statement: Not applicable.

Informed Consent Statement: Not applicable.

Data Availability Statement: The data presented in this study are available on request from the corresponding author. The data are not publicly available due to privacy issues.

Conflicts of Interest: The authors declare no conflicts of interest.

References

1. Sivaranjani, R.; Veerathai, S.; Jeoly Jenifer, K.; Sowmiya, K.; Rupesh, K.J.; Sudalai, S.; Arumnugam, A. A comprehensive review on biohydrogen production pilot scale reactor technologies: Sustainable development and future prospects. *Int. J. Hydrogen Energy* **2023**, *48*, 23785–23820. [CrossRef]
2. Dzogbewu, T.C.; de Beer, D.J. Additive manufacturing of selected ecofriendly energy devices. *Virtial Phys. Prototyp.* **2023**, *18*, e2276245. [CrossRef]
3. Abdin, Z.; Zafaranloo, A.; Rafiee, A.; Mérida, W.; Lipiński, W.; Khalilpour, K.R. Hydrogen as an energy vector. *Renew. Sustain. Energy Rev.* **2020**, *120*, 109620. [CrossRef]
4. Tarhan, C.; Cil, M.A. A study on hydrogen, the clean energy of the future: Hydrogen storage methods. *J. Energy Storage* **2021**, *40*, 102676. [CrossRef]
5. Johnston, B.; Mayo, M.C.; Khare, A. Hydrogen: The energy source for the 21st century. *Technovation* **2005**, *25*, 569–585. [CrossRef]
6. Baroutaji, A.; Wilberforce, T.; Ramadan, M.; Olabi, A.G. Comprehensive investigation on hydrogen and fuel cell technology in the aviation and aerospace sectors. *Renew. Sustain. Energy Rev.* **2019**, *106*, 31–40. [CrossRef]
7. Valverde, L.; Pino, F.J.; Guerra, J.; Rosa, F. Definition, analysis and experimental investigation of operation modes in hydrogen-renewable-based power plants incorporating hybrid energy storage. *Energy Convers. Manag.* **2016**, *113*, 290–311. [CrossRef]
8. Belz, S. A synergetic use of hydrogen and fuel cells in human spaceflight power systems. *Acta Astronaut.* **2016**, *121*, 323–331. [CrossRef]
9. Li, C.; Xu, H.; Bao, C.; Hou, S. Palladium membrane coated with zeolitic armor anchored by diffusion-piling to enhance performance. *ACS Appl. Nano Mater.* **2019**, *2*, 3377–3384. [CrossRef]
10. Ma, Q.; He, Y.; You, J.; Chen, J.; Zhang, Z. Probabilistic risk assessment of fire and explosion of onboard high-pressure hydrogen system. *Int. J. Hydrogen Energy* **2024**, *50*, 1261–1273. [CrossRef]
11. Abohamzeh, E.; Salehi, F.; Sheikholeslami, M.; Abbassi, R.; Khan, F. Review of hydrogen safety during storage, transmission, and applications processes. *J. Loss Prev. Process Ind.* **2021**, *72*, 104569. [CrossRef]
12. Rigas, F.; Sklavounos, S. Evaluation of hazards associated with hydrogen storage facilities. *Int. J. Hydrogen Energy* **2005**, *30*, 1501–1510. [CrossRef]
13. Sangchap, M.; Hashtroudi, H.; Thathsara, T.; Harrison, C.J.; Kingshott, P.; Kandjani, A.E.; Trinchi, A.; Shafiei, M. Exploring the promise of one-dimensional nanostructures: A review of hydrogen gas sensors. *Int. J. Hyodrogen Energy* **2024**, *50*, 1443–1457. [CrossRef]
14. Kim, Y.K.; Hwang, S.-H.; Jeong, S.M.; Son, K.Y.; Lim, S.K. Colorimetric hydrogen gas sensor based on PdO/metal oxides hybrid nanoparticles. *Talanta* **2018**, *188*, 356–364. [CrossRef] [PubMed]
15. Nasir, M.E.; Dickson, W.; Wurtz, G.A.; Wardley, W.P.; Zayats, A.V. Hydrogen detected by the naked eye: Optical hydrogen gas sensors based on core/shell plasmonic nanorod metamaterials. *Adv. Mater.* **2014**, *26*, 3532–3537. [CrossRef] [PubMed]
16. Korotcenkov, G.; Han, S.D.; Stetter, J.R. Review of electrochemical hydrogen sensors. *Chem. Rev.* **2009**, *109*, 1402–1433. [CrossRef] [PubMed]
17. Phan, D.-T.; Chung, G.-S. Surface acoustic wave hydrogen sensors based on ZnO nanoparticles incorporated with a Pt catalyst. *Sens. Actuators B Chem.* **2012**, *161*, 341–348. [CrossRef]
18. Zhang, Y.-N.; Peng, H.; Qian, X.; Zhang, Y.; An, G.; Zhao, Y. Recent advancements in optical fiber hydrogen sensors. *Sens. Actuators B Chem.* **2017**, *244*, 393–416. [CrossRef]

19. Imai, Y.; Tadaki, D.; Ma, T.; Kimura, Y.; Hirano-Iwata, A.; Niwano, M. Response characteristics of hydrogen gas sensor with porous piezoelectric poly(vinylidene fluoride) film. *Sens. Actuators B Chem.* **2017**, *247*, 479–489. [CrossRef]
20. Meng, F.; Shi, X.; Yuan, Z.; Ji, H.; Qin, W.; Shen, Y.B.; Xing, C. Detection of four alcohol homologue gases by ZnO gas sensor in dynamic interval temperature modulation mode. *Sens. Actuators B Chem.* **2022**, *350*, 130867. [CrossRef]
21. Bhowmick, T.; Ghosh, A.; Nag, S.; Majumder, S.B. Sensitive and selective CO_2 gas sensor based on CuO/ZnO bilayer thin-film architecture. *J. Alloys Compd.* **2022**, *903*, 163871. [CrossRef]
22. Ren, X.; Xu, Z.; Liu, D.; Li, Y.; Zhang, Z.; Tang, Z. Conductometric NO_2 gas sensors based on MOF-derived porous ZnO nanoparticles. *Sens. Actuators B Chem.* **2022**, *357*, 131384. [CrossRef]
23. Kong, Y.; Li, Y.; Cui, X.; Su, L.; Ma, D.; Lai, T.; Yao, L.; Xiao, X.; Wang, Y. SnO_2 nanostructured materials used as gas sensors for the detection of hazardous and flammable gases: A review. *Nano Mater. Sci.* **2022**, *4*, 339–350. [CrossRef]
24. Gasso, S.; Sohal, M.K.; Mahajan, A. MXene modulated SnO_2 gas sensor for ultra-responsive room-temperature detection of NO_2. *Sens. Actuators B Chem.* **2022**, *357*, 131427. [CrossRef]
25. Tian, X.; Cui, X.; Lai, T.; Ren, J.; Yang, Z.; Xiao, M.; Wang, B.; Xiao, X.; Wang, Y. Gas sensors based on TiO_2 nanostructured materials for the detection of hazardous gases: A review. *Nano Mater. Sci.* **2021**, *3*, 390–403. [CrossRef]
26. Zhang, D.; Yu, S.; Wang, X.; Huang, J.; Pan, W.; Zhang, J.; Meteku, B.E.; Zeng, J. UV illumination-enhanced ultrasensitive ammonia gas sensor based on (001)TiO_2/MXene heterostructure for food spoilage detection. *J. Hazard. Mater.* **2022**, *423*, 127160. [CrossRef] [PubMed]
27. Li, H.; Wu, C.-H.; Liu, Y.-C.; Yuan, S.-H.; Chiang, Z.-X.; Zhang, S.; Wu, R.-J. Mesoporous WO_3-TiO_2 heterojunction for a hydrogen gas sensor. *Sens. Actuators B Chem.* **2021**, *341*, 130035. [CrossRef]
28. Guo, M.; Luo, N.; Chen, Y.; Fan, Y.; Wang, X.; Xu, J. Fast-response MEMS xylene gas sensor based on CuO/WO_3 hierarchical structure. *J. Hazard. Mater.* **2022**, *429*, 127471. [CrossRef] [PubMed]
29. Katoch, A.; Choi, S.W.; Kim, H.W.; Kim, S.S. Highly sensitive and selective H_2 sensing by ZnO nanofibers and the underlying sensing mechanism. *J. Hazard. Mater.* **2014**, *286*, 229–235. [CrossRef]
30. Katoch, A.; Chou, S.-W.; Kim, J.-H.; Lee, J.H.; Lee, J.-S.; Kim, S.S. Importance of the nanograin size on the H_2S-sensing properties of ZnO–CuO composite nanofibers. *Sens. Actuators B Chem.* **2015**, *214*, 111–116. [CrossRef]
31. Abdullah, F.H.; Abu Bakar, N.H.H.; Abu Bakar, M. Current advancements on the fabrication, modification, and industrial application of zinc oxide as photocatalyst in the removal of organic and inorganic contaminants in aquatic systems. *J. Hazard. Mater.* **2022**, *424*, 127416. [CrossRef] [PubMed]
32. Koga, K. Electronic and catalytic effects of single-atom Pd additives on the hydrogen sensing properties of Co_3O_4 nanoparticle films. *ACS Appl. Mater. Interfaces* **2020**, *12*, 20806–20823. [CrossRef] [PubMed]
33. Sun, X.; Hao, L.; Chen, L.; Guo, X.; Han, C.; Chen, J.; Jiao, W.; Wang, R.; He, X. Spray deposition of colorimetric H_2 detector with Pd/MoO_3 nanocomposites for rapid hydrogen leakage monitoring at room temperature. *Appl. Surf. Sci.* **2022**, *599*, 153878. [CrossRef]
34. Lee, J.-H.; Kim, J.-Y.; Kim, J.-H.; Mirzaei, A.; Kim, H.W.; Kim, S.S. Pd-decorated Si nano-horns as sensitive and selective hydrogen gas sensors. *Mater. Res. Bull.* **2020**, *132*, 110985. [CrossRef]
35. Sun, C.; Liu, H.; Shao, J.; Pan, G.; Yang, X.; Wang, M.; Dong, J.; Zhu, M.; Qi, Y. Au-loaded Zn_2SnO_4/SnO_2/ZnO nanosheets for fast response and highly sensitive TEA gas sensors. *Sens. Actuators B Chem.* **2023**, *376*, 132951. [CrossRef]
36. Liu, L.; Wang, Y.; Guan, K.; Liu, Y.; Li, Y.; Sun, F.; Wang, X.; Zhang, C.; Feng, S.; Zhang, T. Influence of oxygen vacancies on the performance of SnO_2 gas sensing by near-ambient pressure XPS studies. *Sens. Actuators B Chem.* **2023**, *393*, 134252. [CrossRef]
37. Liu, L.; Wang, Y.; Liu, Y.; Wang, S.; Li, T.; Feng, S.; Qin, S.; Zhang, T. Heteronanostructural metal oxide-based gas microsensors. *Microsyst. Nanoeng.* **2022**, *8*, 85. [CrossRef]
38. Kumar, N.; Jasani, J.; Sanvane, Y.; Korvink, J.G.; Sharma, A.; Sharma, B. Unfolding the hydrogen gas sensing mechanism across 2D Pnictogen/graphene heterostructure sensors. *Sens. Actuators B Chem.* **2024**, *399*, 134807. [CrossRef]
39. Galvani, M.; Freddi, S.; Sangaletti, L. Disclosing fast detection opportunities with nanostructured chemiresistor gas sensors based on metal oxides, carbon, and transition netal dichalcogenides. *Sensors* **2024**, *24*, 584. [CrossRef]
40. Lupan, O.; Postica, V.; Hoppe, M.; Wolff, N.; Polonskyi, O.; Pauporté, T.; Viana, B.; Jajérus, O.; Kienle, L.; Faupel, F.; et al. PdO/PdO_2 functionalized ZnO:Pd films for lower operating temperature H_2 gas sensing. *Nanoscale* **2018**, *10*, 14107–14127. [CrossRef]
41. Liu, L.; Liu, C.; Li, S.; Wang, L.; Shan, H.; Zhang, X.; Guan, H.; Liu, Z. Honeycombed SnO_2 with ultra sensitive properties to H_2. *Sens. Actuators B Chem.* **2013**, *177*, 893–897. [CrossRef]
42. Li, Z.; Yan, S.; Wu, Z.; Li, H.; Wang, J.; Shen, W.; Wang, Z.; Fu, Y. Hydrogen gas sensor based on mesoporous In_2O_3 with fast response/recovery and ppb level detection limit. *Int. J. Hydrogen Energy* **2018**, *43*, 22746–22755. [CrossRef]
43. Zhang, Y.; Zeng, W.; Li, Y. NO_2 and H_2 sensing properties for urchin-like hexagonal WO_3 based on experimental and first-principle investigations. *Ceram. Int.* **2019**, *45*, 6043–6050. [CrossRef]
44. Wang, Y.-T.; Whang, W.-T.; Chen, C.-H. Hollow V_2O_5 nanoassemblies for high-performance room-temperature hydrogen sensors. *ACS Appl. Mater. Interfaces* **2015**, *7*, 8480–8487. [CrossRef] [PubMed]
45. Chen, J.; Xu, L.; Li, W.; Gou, X. α-Fe_2O_3 nanotubes in gas sensor and lithium-ion battery applications. *Adv. Mater.* **2005**, *17*, 582–586. [CrossRef]

46. Tonezzer, M.; Iannotta, S. H_2 sensing properties of two-dimensional zinc oxide nanostructures. *Talanta* **2014**, *122*, 201–208. [CrossRef] [PubMed]
47. Chiang, Y.-J.; Li, K.-C.; Lin, Y.-C.; Pan, F.-M. A mechanistic study of hydrogen gas sensing by PdO nanoflake thin films at temperatures below 250 °C. *Phys. Chem. Chem. Phys.* **2015**, *17*, 3039–3049. [CrossRef] [PubMed]
48. Tang, Z.; Zhang, Y.; Deng, X.; Dai, Y.; Zhang, W.; Fan, F.; Qing, B.; Zhu, C.; Fan, J.; Shi, Y. The H_2 sensing properties of facets-dependent Pd nanoparticles-supported ZnO nanorods. *Dalton Trans* **2018**, *47*, 15331–15337. [CrossRef]
49. Choi, S.-J.; Chattopadhyay, S.; Kim, J.J.; Kim, S.-J.; Tuller, H.L.; Rutledge, G.C.; Kim, I.-D. Coaxial electrospinning of WO_3 nanotubes functionalized with bio-inspired Pd catalysts and their superior hydrogen sensing performance. *Nanoscale* **2016**, *8*, 9159–9166. [CrossRef]
50. Sarica, N.; Alev, O.; Arslan, L.C.; Öztürk, Z.Z. Characterization and gas sensing performances of noble metals decorated CuO nanorods. *Thin Solid Films* **2019**, *685*, 321–328. [CrossRef]
51. Peng, Y.; Zheng, L.; Zou, K.; Li, C. Enhancing performances of a resistivity-type hydrogen sensor based on Pd/SnO_2/RGO nanocomposites. *Nanotechnol* **2017**, *28*, 215501. [CrossRef] [PubMed]
52. Zhang, L.; Xie, G.; Liu, F.; Ji, H. High hydrogen selectivity Pd-Ni alloy film hydrogen sensor with hybrid organosilica membranes. *J. Alloys Compd.* **2023**, *941*, 168898. [CrossRef]
53. Kim, S.; Maeng, B.; Yang, Y.; Kim, K.; Jung, D. Hybrid hydrogen sensor based on Pd/WO_3 showing simultaneous chemiresistive and gasochromic response. *Nanomater* **2023**, *13*, 2563. [CrossRef]
54. Gong, J.; Wang, Z.; Tang, Y.; Sun, J.; Wei, X.; Zhang, Q.; Tian, G.; Wang, H. MEMS-based resistive hydrogen sensor with high performance using a palladium-gold alloy thin film. *J. Alloys Compd.* **2023**, *930*, 167398. [CrossRef]
55. TGS 2626-C00-For the Detection of Hydrogen. Available online: https://www.figarosensor.com/product/docs/tgs2616-c00_product%20information(fusa)rev02.pdf (accessed on 30 October 2023).
56. GMV-2021B MEMS H2 Sensor Manual. Available online: https://www.winsen-sensor.com/d/files/manual/gmv-2021b.pdf (accessed on 30 October 2023).